IEEE Access
Multidisciplinary | Rapid Review | Open Access Journal

Received November 1, 2019, accepted November 14, 2019, date of publication November 20, 2019,
date of current version December 5, 2019.

Digital Object Identifier 10.1109/ACCESS.2019.2954551

Gaussian Mixture Learning for LDPC Coded BICM Receivers With Blanking Nonlinearity

YUAN HE[1], (Student Member, IEEE), MING JIANG[1,2], (Member, IEEE), AND CHUNMING ZHAO[1,2], (Member, IEEE)

[1]National Mobile Communications Research Laboratory, Southeast University, Nanjing 210096, China
[2]Purple Mountain Laboratories, Nanjing 210096, China

Corresponding author: Ming Jiang (jiang_ming@seu.edu.cn)

This work was supported in part by the National Science and Technology Projects of China under Grant 2018ZX03001002, in part by the National Natural Science Foundation of China under Grant 61771133, and in part by the National Key Research and Development Program of China under Grant 2018YFB1801103.

ABSTRACT With the aid of blanking nonlinearity, the low density parity check (LDPC) coded bit-interleaved coded modulation (BICM) has been jointly considered as a robust mitigation for the impulsive interference in orthogonal frequency division multiplexing (OFDM) systems. However, the Gaussian assumption for the nonlinear channel conditional probability induces the mismatched L-values in the conventional MAP demodulator. In this paper, combined with the pulse blanking optimization via the PEXIT analysis, we propose a novel MAP demodulator based on the Gaussian mixture model (GMM) and estimate the parameters with the expectation-maximization (EM) algorithm. Taking the L-band Digital Aeronautical Communication System Type1 (L-DACS1) as an example, the GMM-based MAP demodulator can obtain the PEXIT thresholds that match the decoding curves well and provide the better BER performance in the interference-limit channel environment.

INDEX TERMS LDPC code, BICM, blanking nonlinearity, Gaussian mixture model, expectation-maximization algorithm.

I. INTRODUCTION

Orthogonal frequency division multiplexing (OFDM) has been regarded as a high data-rate and bandwidth-efficient technique that is widely adopted in modern wireless communication systems [1], e.g., the L-band digital aeronautical communication system type1 (L-DACS1) for air-to-ground and air-to-air aeronautical communications. However, L-DACS1 systems coexist with legacy systems, such as distance measuring equipment (DME), secondary surveillance radar (SSR) and global navigation satellite system (GNSS) [2]. One drawback of the L-DACS1 system is that it suffers from the impulsive interference caused by the legacy avionic, navigation and surveillance systems, which leads to a severe degradation of system performance [3], [4].

To overcome the impulsive interference, the blanking nonlinearity is an effective method by blanking or clipping the received signals with amplitudes exceeding a predefined threshold, which results in a remarkable improvement [5], [6]. On the other hand, the BICM architecture facilitates to further enhance the error correction capability between the demodulator and the decoder [7]. In this paper, we combine the bit-interleaved coded modulation (BICM) receiver with the blanking nonlinearity, resulting in a promising solution. Taking advantage of a near Shannon limit performance and excellent error correction capability [8], the LDPC-coded BICM receivers are expected to exhibit a significant robustness to the impulsive interference.

Nevertheless, the inter-carrier distortion caused by blanking nonlinearity in maximum *a posteriori* (MAP) demodulator makes error distribution function differ from the Gaussian assumption. The demodulator that designed under Gaussian assumption mismatches the nonlinear channel and suffers from the incorrect soft output, which remains a challenge [9]. To solve the problem, an enhanced demapping algorithm modifies the constellation symbols with the consideration of reconstructed nonlinear distortion to improve the demapping extrinsic log likelihood ratio (LLR), which however consumes numerous complexity [10]. In [11], an approximation of the LLR is derived in the case of α-stable impulsive interferences. In [12], a doubly iterative receiver with pulse blanking is designed to overcome the impulsive interference,

The associate editor coordinating the review of this manuscript and approving it for publication was Md. Fazlul Kader.

including an inner loop and an outer loop. The inner loop between the demodulator and decoder improve the soft information, while the outer loop further enhance the pulse blanking by feeding the soft information back to pulse blanker.

Recently, Gaussian mixture model (GMM) has been used in the areas involving code design, soft demodulation and signal detection etc., due to the power of complex probability density function approximation [13]–[15]. In [15], authors present a theoretical characterization of convolutional coded BICM transmission impaired by the Gaussian mixture noise. So far, there is no research on applying GMM for enhancing robustness of the impulsive interference in the BICM receiver with the blanking nonlinearity. Inspired by the advancements, we propose a novel MAP demodulator based on the GMM in the LDPC coded BICM receiver, taking into account the characteristic of blanking nonlinearity. Since there lacks a mathematically tractable model for the error distribution function, the GMM offers a powerful ability of fitting. Major contributions of this paper lie in:

- Considering the influence of LDPC codes, we investigate the threshold optimization for pulse blanking using the modified protograph based extrinsic information transfer (PEXIT) analysis. The relationship between the optimal blanking threshold and coded modulation schemes is analytically discussed in various interference scenarios.
- Selecting an optimal threshold, we improve the MAP demodulator by fitting the channel conditional probability as the GMM, resulting in a revised LLR criterion. Under the assumption of GMM distribution, we obtain the associated parameters by using the expectation-maximization (EM) algorithm.

With the fine-tuned parameters off-line, the GMM-based demapper costs no extra computational complexity and obtains the more accurate soft outputs to achieve an increasing performance gain.

The remainder of this paper is organized as follows. In Section II, we propose an LDPC coded BICM receiver with blanking nonlinearity over the impulsive interference channel. After that, the modified PEXIT analysis is utilized to investigate the blanking threshold optimization for the various coding modulation schemes. Then, we propose an enhanced GMM-based demodulator with EM learning algorithm in Section III. In the comparison of PEXIT analysis, we give an example of the L-DACS1 system and demonstrate the simulation results of the GMM-based LDPC-coded BICM receiver with pulse blanking in Section IV. Conclusions are drawn in Section V. The list of abbreviations about terminologies is summarized in Table 1.

TABLE 1. List of abbreviations about terminologies in this paper.

Abbreviation	Definition
L-DACS1	L-band Digital Aeronautical Communication System Type1
DME	Distance Measuring Equipment
dBm	Decibels above one milliwatt
ppps	Pulse pair per second
RS-CC	Reed-Solomon codes combined with convolutional codes
WiMAX	IEEE 802.16 standard for wireless access systems
AR4A	Accumulate repeat accumulate LDPC code with repetition-4
GF	Galois field
PEG	Progressive-edge-growth method for the LDPC construction
BG2	Base graph designed for the 5G LDPC code

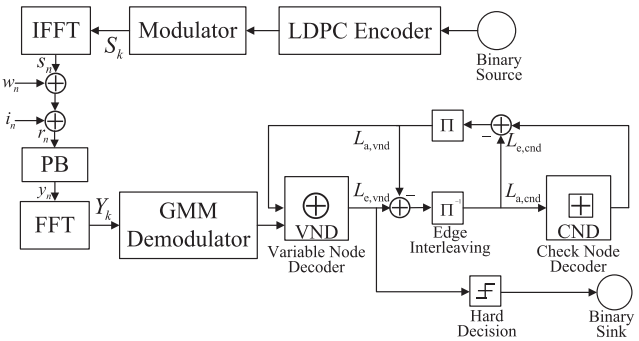

FIGURE 1. Block diagram of LDPC-coded BICM system with pulse blanking.

II. SYSTEM MODEL

The BICM receiver with blanking nonlinearity in an LDPC-coded OFDM system is depicted in Fig. 1. At the transmitter, the information bits are coded and mapped into the modulated symbols $[S_0, S_1, \ldots, S_{N-1}]^T$ after the LDPC encoder with the code rate R and the 2^M-ary constellation modulator. Then, the modulation symbols are fed to an N point inverse fast Fourier transform (N-IFFT) converter to generate the time domain signals $[s_0, s_1, \ldots, s_{N-1}]^T$, as follows

$$s_n = \frac{1}{\sqrt{N}} \sum_{k=0}^{N-1} S_k e^{j\frac{2\pi nk}{N}}, \quad n, k = 0,\ 1,\ \ldots,\ N-1 \quad (1)$$

where k denotes the subcarrier index, and n is the sample index. The transmitted signals $\left[s_0, s_1, \ldots, s_{N+N_{CP}-1}\right]^T$ are finally completed after the insertion of the cyclic prefix of length N_{CP} and the transmit power is normalized to unity.

Considering the impulsive interference, the received signal r_n with perfect timing and synchronization can be modeled by summing the mutually independent interference i_n and the additive white Gaussian noise (AWGN) w_n with zero mean and variance σ_n^2

$$r_n = s_n + w_n + i_n, \quad n = 0, 1, \ldots, N-1. \quad (2)$$

At the receiver, the BICM system combined with blanking nonlinearity is an effective scheme to eliminate the impulsive interference. Specifically, the signals suffering from the impulsive interference are set to zero by the method of pulse blanking when their amplitudes exceed the blanking threshold. The blanked signals $[y_0, y_1, \ldots, y_{N-1}]^T$ can be

expressed as

$$y_n = \begin{cases} r_n, & if\ |r_n| < T_B \\ 0, & otherwise \end{cases} \tag{3}$$

where T_B is the pulse blanking threshold.

The LDPC-coded BICM architecture can be viewed as a serial concatenation with an MAP demodulator and an outer LDPC decoder. The conventional MAP demodulator is employed with the frequency-domain symbols with blanking nonlinearity $[Y_0, Y_1, \ldots, Y_{N-1}]^T$ after the N point fast Fourier transform (N-FFT). With considering the nonlinear distortion, the log-likelihood ratio (LLR) value $L_{e,dem}(S_k^m)$ on the m-th bit is calculated and fed into the decoder to estimate the transmitted message bit by

$$\begin{aligned} L_{e,dem}(S_k^m) &= \log \frac{\sum\limits_{S_k^m \in \chi_1^m} p(Y_k|S_k)}{\sum\limits_{S_k^m \in \chi_0^m} p(Y_k|S_k)} \\ &= \max_{S_k^m \in \chi_1^m} \{\log p(Y_k|S_k)\} - \max_{S_k^m \in \chi_0^m} \{\log p(Y_k|S_k)\} \end{aligned} \tag{4}$$

where χ_b^m denotes the constellation subset with the m-th bit $b = 0, 1$, S_k^m stands for the m-th bit on the constellation label with the k-th subcarrier and $p(Y_k|S_k) \sim \mathcal{N}(0, \sigma_n^2)$ equals to the Gaussian distribution [16].

The MAP demodulator delivers the $L_{e,dem}$ to the *a priori* input $L_{a,dec}$ of the LDPC decoder by passing through the random interleaver. The iterative decoding for LDPC codes can be viewed as a serial concatenation with an inner variable-node decoder (VND) and an outer check-node decoder (CND). Each VND has d_v messages from an edge interleaver and one message from demodulation, so the extrinsic LLR output $L_{e,vnd}^i$ in the i-th variable node is computed by summing $d_v - 1$ *a priori* LLR inputs from other variable nodes and the channel observation $L_{dem}^{k,m}$ from the demodulator, .i.e.,

$$L_{e,vnd}^i = L_{dem}^{k,m} + \sum_{j=1, j\neq i}^{d_v} L_{a,vnd}^j. \tag{5}$$

Then, the extrinsic LLR output $L_{e,dec}$, which is computed by the iterative belief propagation decoder, would feed back to the MAP demodulator as the *a priori* value $L_{a,dem}$ [17]. The extrinsic LLRs continue to update iteratively between the demodulator and decoder to form the final decisions until all the parity-check equations are satisfied or the maximum number of iterations is reached.

III. BICM RECEIVER WITH GAUSSIAN MIXTURE LEARNING

According to Section II, we address the BICM receiver design for the LDPC coded OFDM systems to combat the blanking nonlinearity over the impulsive interference channel. However, there are still two key issues on the mitigation of nonlinearity distortion, i.e., the blanking threshold optimization and the extrinsic LLR correction. Considering the impact of the LDPC coding scheme, it is important to explore the blanking threshold optimization. Meanwhile, with the optimized blanking threshold, the demodulator shall be redesigned to concern the inter-carrier distortion caused by blanking nonlinearity, which can provide more accurate extrinsic LLRs to enhance the demapping performance. Here, we search the optimal threshold via the modified protograph based extrinsic information transfer (PEXIT) chart. Additionally, we develop an enhanced GMM-based demodulator with EM learning algorithm, based on the optimized threshold evaluated by the PEXIT analysis.

A. PULSE BLANKING OPTIMIZATION

Compared with other analytical solutions of blanking threshold that maximize SINR [12], [18], the modified PEXIT chart provides a visualized and more accurate tool to optimize the thresholds regarding the structures of protograph-based LDPC codes. Due to the pulse blanking over impulsive interference channel, we revise the PEXIT analysis that is similar to [19] except the initialization step at the output of MAP demodulator [20]. In this way, the modified PEXIT analysis can provide the optimized blanking value by searching for the lowest decoding threshold of the LDPC decoder with different pulse blanking thresholds. The pulse blanking with the lowest decoding threshold corresponds to the optimal blanking value for our threshold analysis method. Here, let γ denote the E_b/N_0, which is the ratio of average OFDM signal power to the noise power per bit. The decoding threshold γ^* is defined as the minimum required E_b/N_0 that the *a posteriori* mutual information (MI) can converge to 1. The proposed PEXIT analysis is given as follows.

- **Initialization**
  Select an initial value of γ. Set $I_{a,vnd}^{i,j} = 0$, which is the incoming *a priori* MI from the i-th variable node to the j-th check node. Initialize the *a priori* MI of MAP demodulator $I_{a,dem}^{k,m} = 0$.
- **Extrinsic MI calculation of demodulator**
  Compute the extrinsic MI of the demodulator $I_{e,dem}^{k,m}$, which is the MI between S_k and $L_{dem}^{k,m}$ over impulsive interference channel with pulse blanking. The samples of $L_{dem}^{k,m}$ are derived by equation (9).
- **Channel MI from variable nodes**
  The channel MI of the i-th variable node I_{ch}^i is obtained by setting $I_{ch}^i = I_{e,dem}^{k,m}$ except $I_{ch}^i = 0$ when the variable node is punctured.
- **MI updating between variable nodes and check nodes**
  The MI updating in LDPC decoder includes the variable-node to check-node updating and the check-node to variable-node updating. Then the MI is iteratively updated between the variable nodes and check nodes until the MI converges to 1, where the detailed steps are shown in [19]. The decoding threshold γ^* can be obtained by searching the lowest threshold leading to convergence via the dichotomic method.

TABLE 2. The DME interference scenarios for the L-band digital aeronautical communication system Type1.

Case	Transmit Power	Rate
1	43 dBm	3600 ppps
2	49 dBm	3600 ppps
3	43 dBm	7200 ppps
4	49 dBm	7200 ppps
5	53 dBm	7200 ppps

- **Blanking Threshold Optimization**
  By using the modified PEXIT analysis for a protograph-based LDPC code, we calculate the decoding thresholds $\gamma^*(T_B)$ corresponding to all the possible blanking T_B. The optimal blanking value T_B^* leads to the lowest decoding threshold $\gamma^*(T_B)$, .i.e.,

$$T_B^* = \arg\min_{T_B} \gamma^*(T_B). \tag{6}$$

To investigate the threshold optimization of pulse blanking, we carry out the PEXIT analysis on the LDPC coded L-DACS1 system with pulse blanking over the impulsive DME interference channel. The DME signal is the main interference from the legacy systems, which is modeled by the pairs of Gaussian-shaped pulses. It can be mathematically described by

$$i_n = \exp(-\frac{\alpha n^2 t_s^2}{2}) + \exp(-\frac{\alpha(nt_s - \Delta t)^2}{2}) \tag{7}$$

where $\alpha = 4.5 \cdot 10^{11} s^{-2}$ is a constant that determines the pulse width, t_s is the sampling interval with 1.6 μs and Δt is the interval between pulse pairs that satisfies 12 or 36 μs [2]. We focus on five DME interference scenarios, as illustrated in Table 2 and the transmit power for L-DACS1 is set to 43 dBm. The corresponding scenarios denote that the DME signals are transmitted by the specific pairs per second with the transmit peak power and these candidate scenarios exhibit various combinations of DME transmit power and transmission rate. Moreover, we select the rate-2/3 5G LDPC code, in which the tanner graph is designed via the second base-graph (BG2) with lifting size 160.

Assuming that the maximum number of iterations is 1000, and the precision accuracy of PEXIT analysis is 1e-4, Fig. 2 illustrates the decoding thresholds $\gamma^*(T_B)$ corresponding to different DME interference scenarios of the LDPC coded OFDM systems for the different modulations with Gray mapping. The modulation constellations involve the 16QAM, 64QAM and 256QAM, respectively. We remark that the PEXIT requires on-line computation with noticeable complexity, while the blanking threshold used in the practical receiver can be optimized off-line. It can be observed that each arrow points to the corresponding optimal blanking threshold T_B^* in a case with specific modulation. Due to the trade-off between the impulsive interference mitigation and the system performance as we discussed in Section I, the lower blanking threshold suffers more distortion of

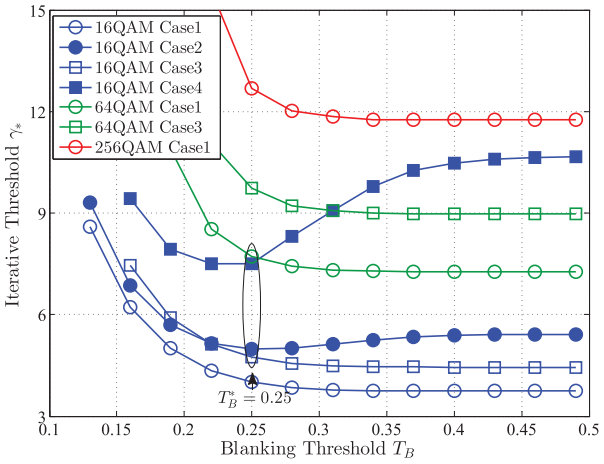

FIGURE 2. PEXIT chart of the LDPC coded OFDM systems with different modulations and DME interference scenarios.

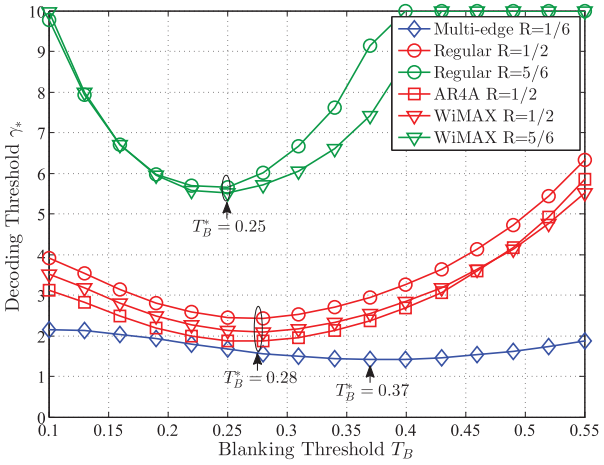

FIGURE 3. PEXIT analysis of various LDPC coding schemes with QPSK modulation in interference scenario Case5.

blanked OFDM signals, while the higher value causes noticeable degradation by the remaining DME interference. Both two points deteriorate the decoding performance. As a consequence, the decoding threshold curve of 16QAM modulation becomes the convex function when the interference scenario is Case2 or Case4, resulting in an optimal blanking threshold that minimizes the convergence threshold. The curves of other cases present non-convex function, which allows the optimal blanking threshold larger than the value $T_B = 0.34$.

To investigate the impact of code rate and protograph structure, Fig. 3 shows the PEXIT results of the LDPC coded OFDM systems with QPSK in Case5 scenario. We choose some LDPC codes which can be described by simple protographs, such as the multi-edge LDPC codes [21], the regular LDPC codes, the LDPC codes in WiMAX [22] and the AR4A codes [23]. Specifically, we select a rate-1/6 multi-edge LDPC code designed via lifting by the improved PEG construction [24], and the protograph in [21] is optimized under the consideration of the decoding threshold and error floor [25]. A rate-1/2 regular LDPC code is constructed by

PEG algorithm from a regular protograph, where one check-node is connected with two variable nodes via three edges, respectively. Besides, a rate-5/6 regular LDPC code similar to the rate-1/2 one is used here, which can be represented by a regular graph consisting of one check-node and six degree-3 variable nodes. WiMAX LDPC codes are structured LDPC codes defined by base matrices, which also can be mapped into equivalent protographs. AR4A code is the rate-1/2 punctured irregular repeat-accumulate code defined by the protograph in [23]. The coded block lengths of WiMAX LDPC codes and the others are set to 2304 and 2400. Each arrow points to the corresponding optimal blanking threshold T_B^*. Due to a trade-off between the impulsive interference mitigation and the system performance as we discussed in Section I, there exists an optimal blanking threshold that minimizes the convergence threshold of the overall LDPC coded system.

On the other hand, the optimal blanking thresholds vary with the code rates, but are not relevant to the protograph structures. As seen from the results in Fig. 3, the optimal values for the AR4A code and the WiMAX code with code rate 1/2 both are 0.28, which is the same as that of the rate-1/2 regular code. Meanwhile, these rate-1/2 protograph-based LDPC codes have the different decoding thresholds γ^* in spite of the same optimal blanking threshold. It can also be implied that the optimal blanking threshold for the low-rate LDPC code is higher than the high-rate one. Namely, the optimal value for the rate-1/6 multi-edge LDPC code is higher than the rate-1/2 and rate-5/6 ones. In this case, the low-rate coding schemes can compensate for the more serious inter-carrier interference caused by the higher blanking threshold since their error correction capabilities are much better than those of high-rate codes.

B. MAP DEMODULATOR WITH EM ALGORITHM

In the MAP demodulator with AWGN assumption, the extrinsic LLR $L_{e,dem}(S_k^m)$ on the k-th subcarrier is calculated by the Max-Log-MAP algorithm separately. In the context of DME interference, the blanking nonlinearity causes a serious nonlinearity distortion, which could be regarded as a mixture of remaining impulsive interference and inter-carrier interference. Such a nonlinearity impairment induces severe performance degradation of the BICM receiver and the nonlinear model should be utilized to characterize the conditional probability with respect to $p(Y_k|S_k)$.

It was claimed that the GMM can be used to characteristic the non-Gaussian error probability distribution after nonlinear channel equalization [14]. Such a Gaussian mixture learning with EM algorithm subjects to the machine learning (ML), which has attracted increasing attention in the physical layer communications [26]–[29]. Thus, we establish the GMM to fit the nonlinearity distortion $p(Y_k|S_k)$ conditioned on the training sequence z_k. In the GMM-based BICM scheme, we propose an EM algorithm for MAP demodulation (EM-MAP) to learn the parameters and output the correction of extrinsic LLRs.

Specifically, we model the channel conditional probability $p(Y_k|S_k)$ as the GMM with J Gaussian components, i.e.,

$$p_{Y_k|S_k}(x^{(i)};\delta,\mu,\Sigma)=\sum_{j=1}^{J}\delta_j\mathcal{N}_{Y_k|S_k}(x^{(i)};\mu_j,\Sigma_j) \tag{8}$$

where the mixing proportion parameters equal to $\sum_{j=1}^{J}\delta_j=1$ and $\mathcal{N}(x^{(i)};\mu_j,\Sigma_j)$ denotes the j-th Gaussian probability density function with mean μ_j and variance Σ_j. Basically, the GMM parameter estimation within MAP demodulator suffers from high computational complexity that is impractical in application. Then, we train the error samples x for Y_k on the condition S_k and resort to the EM-MAP algorithm. The EM-MAP algorithm is an unsupervised learning method that automatically estimates the corresponding GMM parameters by searching the maximization of log likelihood function,

$$\ell(\delta,\mu,\Sigma)=\sum\nolimits_{i=1}^{L}\log p_{Y_k|S_k}(x^{(i)};\delta,\mu,\Sigma). \tag{9}$$

Owing to latent variables $z^{(i)}$, the suboptimal EM-based solution of GMM fitting can be asymptotically searched by iteratively performing between the expectation and maximization step. The detailed procedures are summarized as follows.

- **Initialization**
  Select a serial of the initial estimates of parameters, such as the proportion coefficient δ, mean μ and variance Σ. At the first iteration, the Initial extrinsic LLR values of the GMM-based MAP demodulator can be defined as

$$\begin{aligned}
&L_{e,dem}^{(0)}(S_k^m)\\
&\quad=\log\frac{\sum\limits_{S_k^m\in\chi_1^m}p(Y_k|S_k)}{\sum\limits_{S_k^m\in\chi_0^m}p(Y_k|S_k)}\\
&\quad=\log\frac{\sum\limits_{S_k^m\in\chi_1^m}\sum\limits_{j=1}^{J}\delta_j\mathcal{N}_{Y_k|S_k}(x^{(i)};\mu_j,\Sigma_j)}{\sum\limits_{S_k^m\in\chi_0^m}\sum\limits_{j'=1}^{J}\delta_{j'}\mathcal{N}_{Y_k|S_k}(x^{(i)};\mu_{j'},\Sigma_{j'})} \qquad (10)\\
&\quad\approx\max_{S_k^m\in\chi_1^m,j}\{\log(\delta_j\mathcal{N}_{Y_k|S_k}(x^{(i)};\mu_j,\Sigma_j))\}\\
&\qquad-\max_{S_k^m\in\chi_0^m,j'}\{\log(\delta_{j'}\mathcal{N}_{Y_k|S_k}(x^{(i)};\mu_{j'},\Sigma_{j'}))\}. \qquad (11)
\end{aligned}$$

- **Expectation step**
  We calculate the conditional log-likelihood expectation function $\omega_j^{(i)}$ belonging to the j-th GMM component of the observation $x^{(i)}$ with the given latent variable $z^{(i)}$ and the GMM parameters are estimated by

$$\omega_j^{(i)}=p_{Y_k|S_k}(z^{(i)}=j|x^{(i)};\delta,\mu,\Sigma). \tag{12}$$

- **Maximization step**
  In the maximization step, the updated parameters that maximizes log-likelihood expectation are computed as the gradient-based estimates conditioned on latent variable $z^{(i)}$ and observation $x^{(i)}$ in the previous expectation

step, as follows

$$\delta_j = \frac{\sum_{i=1}^{L} \omega_j^{(i)}}{L} \tag{13}$$

$$\mu_j = \frac{\sum_{i=1}^{L} \omega_j^{(i)} x^{(i)}}{\sum_{i=1}^{L} \omega_j^{(i)}} \tag{14}$$

$$\Sigma_j = \frac{\sum_{i=1}^{L} \omega_j^{(i)} \left(x^{(i)} - \mu_j\right)\left(x^{(i)} - \mu_j\right)^T}{\sum_{i=1}^{L} \omega_j^{(i)}}. \tag{15}$$

The algorithm is accomplished until the estimates converge. Considering the effect of blanking nonlinearity, we use training sets to estimate the parameters by the EM-MAP algorithm. Then, we obtain the extrinsic $L_{e,dem}(S_k^m)$ based on the GMM according to the equation (7) to improve the decoding performance of the LDPC-coded BICM receiver. After the optimization of parameter tuning, the GMM-based BICM receiver can fix the parameters in the following to reduce the computational complexity.

C. COMPLEXITY ANALYSIS

Here, we consider the complexity analysis and comparison of the enhanced demodulator with Gaussian mixture learning and the conventional scheme with Max-Log-MAP algorithm. It is noteworthy that the GMM parameter estimation with EM algorithm has been conducted off-line, whose complexity can be ignored. Hence, we focus on the calculation of the extrinsic LLR $L_{e,dem}$ in the MAP demodulator, which is directly related to complexity comparison for both two demapping schemes. For the standard MAP demodulator, the calculation of $L_{e,dem}$ in equation (7) requires a complexity on the order of $\mathcal{O}(2^M)$, since the channel conditional probability $p(Y_k|S_k)$ needs 2^M times Euclidean distance calculations for all the 2^M constellation points [30]. Moreover, the maximization operation involves $2^M - 2$ comparisons, which is the same as that of the GMM-based demodulator. Nevertheless, the proposed scheme has a similar complexity compared with the standard MAP demodulator. The reason is that the Euclidean distance calculation increases linearly with the number of Gaussian components J, whose complexity remains the order of $\mathcal{O}(2^M)$ under the assumption of J components. Meanwhile, the number of complex multiplication in the GMM-based demodulator is $J(2^M + 1/2)$. Besides 2^M Euclidean distance calculations of GMM with J Gaussian components, the real multiplications of J mixing proportion parameters can be calculated as $J/2$ complex multiplications. Hence, the EM-MAP has a slightly larger number of complex multiplications than that of the MAP demodulator [31].

IV. SIMULATION RESULTS

In this section, the GMM-based BICM receiver with blanking nonlinearity is tested in the LDPC coded L-DACS1 system to verify the performance. L-DACS1 is a promising candidate for the L band continental data link proposed by the European Organization for the Safety of Air Navigation (EUROCONTROL) and Federal Aviation Administration (FAA). It employs the frequency division duplex (FDD) configuration and OFDM modulation with 64 subcarriers [1]. The channel bandwidth is 625 kHz and the total symbol duration is 120 μs, including the OFDM symbol of 102.4 μs and cyclic prefix of 17.6 μs. We set the received power and transmission rate of the DME signals according to interference scenarios in Table 2. More details about the L-DACS1 proposal and L-band interference scenarios are summarized in [32].

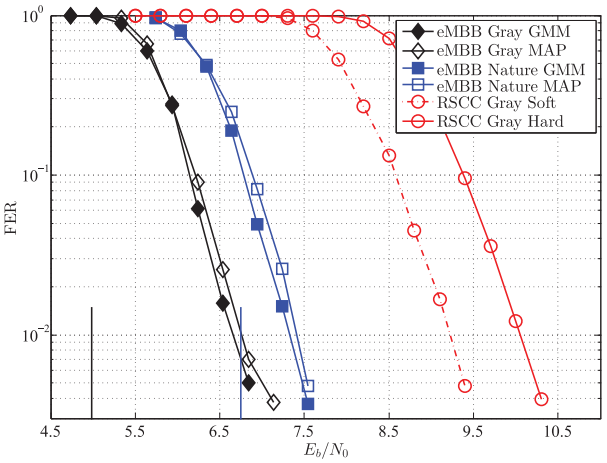

FIGURE 4. FER comparison between the GMM-based LDPC-coded BICM and conventional design for 16QAM with the optimal threshold (Case2).

For the cell-specific adaptive coding and modulation (ACM) mode, L-DACS1 supports the combination of the candidate modulations and a concatenated RS-CC coding scheme, which uses the Reed-Solomon (RS) codes and convolutional codes (CC) as the outer code and inner code, respectively [33]. Considering 64QAM with the rate-3/4 punctured RS-CC code as an example, the parameters of RS code is set to (n=228, k=206) over GF(8) and the polynomial of CC is $(171, 133)_o$ respectively, resulting in a length 4884 coded bits with overall rate 0.68 after the random interleaver. For comparison, the rate-2/3 LDPC code (BG2) with length 4800 and 16QAM with Gray and nature labelling are employed, which achieves the same spectral efficiency with the RS-CC coding scheme. The belief propagation decoding of LDPC codes is used and the maximum number of iterations is set to 50. In the GMM, we choose the number of Gaussian component as $J = 2$ and training error samples with the length of 2000.

Fig. 4 illustrates the frame error rate (FER) comparisons of GMM-based LDPC-coded BICM receiver and the conventional design with 16QAM. The DME ground interrogator sends the DME interference with the transmit power 49 dBm by 3600 pulse pairs per second. By adopting the modified PEXIT analysis, the optimized blanking threshold equals to 0.28. The rate-2/3 5G LDPC code is considered here and the simulations are respectively carried out with different constellation mappings shown in the legend, such as nature mapping and Gray mapping. Besides, the conventional RS-CC

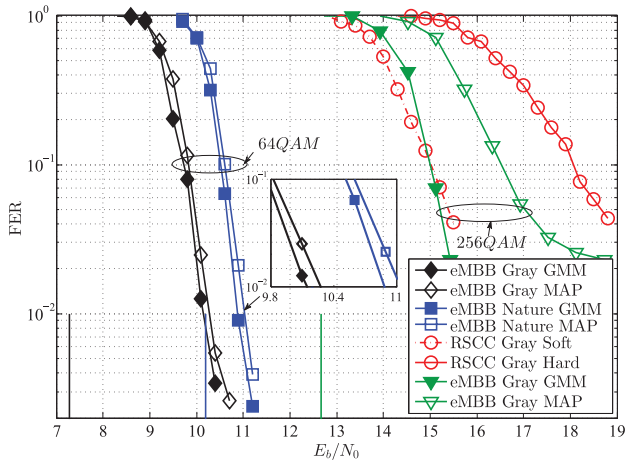

FIGURE 5. FER comparison between the GMM-based LDPC-coded BICM and conventional design for 64QAM and 256QAM with the optimal threshold (Case1).

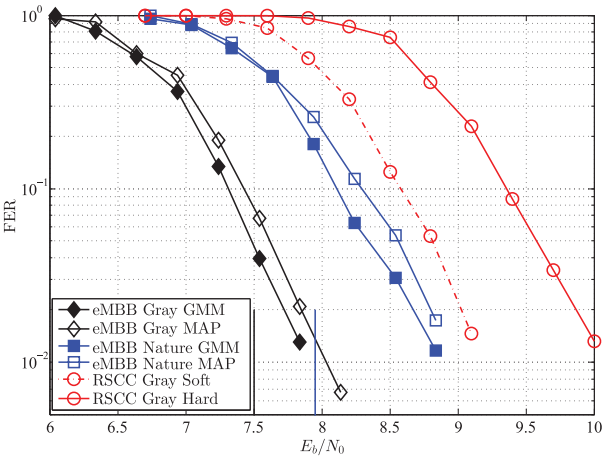

FIGURE 6. FER comparison between the GMM-based LDPC-coded BICM and conventional design for 16QAM with the optimal threshold (Case4).

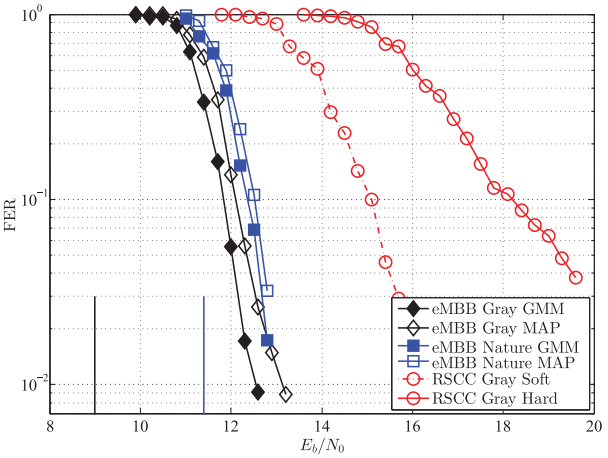

FIGURE 7. FER comparison between the GMM-based LDPC-coded BICM and conventional design for 64QAM with the optimal threshold (Case3).

coding schemes with soft decision and hard decision are given as reference. It can be observed that the GMM-based receiver outperforms the conventional design by about 0.2 dB and 0.3 dB no matter for the Gray and Nature mapping, which demonstrates that our GMM-based BICM receiver can achieve a noticeable performance gain. The benefits will be more obvious as the E_b/N_0 increases, which indicates that the GMM-based MAP demodulator can give more accurate soft information.

In Fig. 5, we present the FER performances of GMM-based LDPC-coded BICM receiver with the 64QAM and 256QAM. The power and transmission rate for the DME interference are 43 dBm and 3600 ppps, respectively. By choosing the optimized threshold as 0.5 via the modified PEXIT analysis, GMM-based BICM receivers obtain different gains by about 0.4 and 1.9 dB over the conventional schemes at a FER of 1e-1 for 64QAM and 256QAM, respectively. The performance gap increases with the increasing modulation order, which indicates that the proposed receiver works better with higher order modulation. Obviously, neither the Nature or Gary mapping, the GMM-based design shows a significant performance gain by more than 7 dB over the standard RS-CC design at a FER of 1e-1. Even though a similar BER performance is shown, the spectral efficiency of LDPC code with 256QAM is higher than that of RS-CC with 64 QAM.

Fig. 6-7 show the impact of DME interference on the GMM-based BICM receiver for the LDPC-coded L-DACS1 system. The scenario Case3 and Case4 are more serious by selecting the pair of transmit power and rate as 43 dBm / 7200ppps and 53 dBm / 7200 ppps, respectively. We can see that the GMM-based BICM receiver exhibit a robustness compared with the counterparts by maintaining the FER performance gains. Specifically, the GMM-based BICM receiver outperforms the conventional scheme by 0.2 and 0.5 dB at a BER of 5e-2 for 16QAM with Gray and Nature mapping in the scenario Case4, while the performance gains for 64QAM equal to 0.5 and 0.2 dB in the scenario Case3 accordingly. The decoding thresholds are marked at the bottom of this figure. Besides, it shows that the FER gap is approaching closely to the gap between the decoding thresholds in Fig. 2 no matter whether the Gray or Nature mapping. The simulation results demonstrate that the modified PEXIT gives an efficient and accurate analysis for the blanking threshold.

V. CONCLUSION

In this paper, we propose an enhanced GMM-based LDPC-coded BICM receiver with blanking nonlinearity to combat the impulsive interference. We optimize the blanking threshold via the modified PEXIT analysis and improve the MAP demodulator by fitting the conditional distribution as the GMM. Under the Gaussian mixture assumption, the EM algorithm is utilized to estimate the parameters accordingly. Simulation results and PEXIT analysis both show that the GMM-based BICM scheme can match the convergence threshold well and achieve a significant improvement.

REFERENCES

[1] M. Schnell, U. Epple, D. Shutin, and N. Schneckenburger, "LDACS: Future aeronautical communications for air-traffic management," *IEEE Commun. Mag.*, vol. 52, no. 5, pp. 104–110, May 2014.

[2] U. Epple and M. Schnell, "Overview of legacy systems in L-band and its influence on the future aeronautical communication system LDACS1," *IEEE Aerosp. Electron. Syst. Mag.*, vol. 29, no. 2, pp. 31–37, Feb. 2014.

[3] J. D. Laster and J. H. Reed, "Interference rejection in digital wireless communications," *IEEE Signal Process. Mag.*, vol. 14, no. 3, pp. 37–62, May 1997.

[4] U. Epple, K. Shibli, and M. Schnell, "Investigation of blanking nonlinearity in OFDM systems," in *Proc. IEEE Int. Conf. Commun. (ICC)*, Jun. 2011, pp. 1–5.

[5] S. V. Zhidkov, "Performance analysis and optimization of OFDM receiver with blanking nonlinearity in impulsive noise environment," *IEEE Trans. Veh. Technol.*, vol. 55, no. 1, pp. 234–242, Jan. 2006.

[6] U. Epple, D. Shutin, and M. Schnell, "Mitigation of impulsive frequency-selective interference in OFDM based systems," *IEEE Wireless Commun. Lett.*, vol. 1, no. 5, pp. 484–487, Oct. 2012.

[7] H. H. Nguyen and T. Q. Bui, "Bit-interleaved coded modulation with iterative decoding in impulsive noise," *IEEE Trans. Power Del.*, vol. 22, no. 1, pp. 151–160, Jan. 2007.

[8] S. A. Basharat and Y. V. Rao, "Design and performance of LDPC codes for OFDM based aeronautical communication systems," in *Proc. 3rd Adv. Int. Conf. Telecommun. (AICT)*, May 2007, p. 24.

[9] A. Martinez, A. G. I. Fabregas, G. Caire, and F. M. J. Willems, "Bit-interleaved coded modulation revisited: A mismatched decoding perspective," *IEEE Trans. Inf. Theory*, vol. 55, no. 6, pp. 2756–2765, Jun. 2009.

[10] J. Tan, Z. Wang, Q. Wang, and L. Dai, "BICM-ID scheme for clipped DCO-OFDM in visible light communications," *Opt. Express*, vol. 24, no. 5, pp. 4573–4581, 2016.

[11] V. Dimanche, A. Goupil, L. Clavier, and G. Gelle, "On detection method for soft iterative decoding in the presence of impulsive interference," *IEEE Commun. Lett.*, vol. 18, no. 6, pp. 945–948, Jun. 2014.

[12] Q. Li, J. Zhang, and U. Epple, "Design and exit chart analysis of a doubly iterative receiver for mitigating impulsive interference in OFDM systems," *IEEE Trans. Commun.*, vol. 64, no. 4, pp. 1726–1738, Apr. 2016.

[13] B. Lu, G. Yue, and X. Wang, "Performance analysis and design optimization of LDPC-coded MIMO OFDM systems," *IEEE Trans. Signal Process.*, vol. 52, no. 2, pp. 348–361, Feb. 2004.

[14] X. Lyu, W. Feng, R. Shi, Y. Pei, and N. Ge, "Artificial neural network-based nonlinear channel equalization: A soft-output perspective," in *Proc. 22nd Int. Conf. Telecommun. (ICT)*, Apr. 2015, pp. 243–248.

[15] A. Kenarsari-Anhari and L. Lampe, "Performance analysis for BICM transmission over Gaussian mixture noise fading channels," *IEEE Trans. Commun.*, vol. 58, no. 7, pp. 1962–1972, Jul. 2010.

[16] S. T. Brink, "Convergence behavior of iteratively decoded parallel concatenated codes," *IEEE Trans. Commun.*, vol. 49, no. 10, pp. 1727–1737, Oct. 2001.

[17] D. J. C. MacKay, "Good error-correcting codes based on very sparse matrices," *IEEE Trans. Inf. Theory*, vol. 45, no. 2, pp. 399–431, Mar. 1999.

[18] U. Epple and M. Schnell, "Adaptive threshold optimization for a blanking nonlinearity in OFDM receivers," in *Proc. IEEE Global Commun. Conf. (GLOBECOM)*, Dec. 2012, pp. 3661–3666.

[19] G. Liva and M. Chiani, "Protograph LDPC codes design based on exit analysis," in *Proc. IEEE Global Telecommun. Conf.*, Nov. 2007, pp. 3250–3254.

[20] Y. He, M. Jiang, X. Wu, and C. Zhao, "Performance analysis and optimization for LDPC coded OFDM systems with pulse blanking," in *Proc. IEEE Wireless Commun. Netw. Conf. (WCNC)*, Apr. 2018, pp. 1–5.

[21] T. Richardson and R. Urbanke, "Multi-edge type LDPC codes," in *Proc. IEEE Inf. Symp. Inform. Theory (ISIT)*, 2002, pp. 24–25.

[22] *IEEE Standard For Local And Metropolitan Area Networks Part 16*, IEEE Standard 802.16e/D12, 2005.

[23] D. Divsalar, S. Dolinar, and C. Jones, "Low-rate LDPC codes with simple protograph structure," in *Proc. Int. Symp. Inf. Theory (ISIT)*, Sep. 2005, pp. 1622–1626.

[24] H. Xiao and A. H. Banihashemi, "Improved progressive-edge-growth (PEG) construction of irregular LDPC codes," *IEEE Commun. Lett.*, vol. 8, no. 12, pp. 715–717, Dec. 2004.

[25] T. V. Nguyen and A. Nosratinia, "Rate-compatible short-length protograph LDPC codes," *IEEE Commun. Lett.*, vol. 17, no. 5, pp. 948–951, May 2013.

[26] T. Wang, C.-K. Wen, H. Wang, F. Gao, T. Jiang, and S. Jin, "Deep learning for wireless physical layer: Opportunities and challenges," *China Commun.*, vol. 14, no. 11, pp. 92–111, 2017.

[27] S. Dörner, S. Cammerer, J. Hoydis, and S. T. Brink, "Deep learning based communication over the Air," *IEEE J. Sel. Topics Signal Process.*, vol. 12, no. 1, pp. 132–143, Feb. 2018.

[28] E. Nachmani, E. Marciano, L. Lugosch, W. J. Gross, D. Burshtein, and Y. Be'ery, "Deep learning methods for improved decoding of linear codes," *IEEE J. Sel. Topics Signal Process.*, vol. 12, no. 1, pp. 119–131, Feb. 2018.

[29] P. Dong, H. Zhang, and G. Y. Li, "Machine learning prediction based CSI acquisition for FDD massive MIMO downlink," in *Proc. IEEE Global Commun. Conf. (GLOBECOM)*, Dec. 2018, pp. 1–6.

[30] J. Tan, Q. Wang, C. Qian, Z. Wang, S. Chen, and L. Hanzo, "A reduced-complexity Demapping algorithm for BICM-id systems," *IEEE Trans. Veh. Technol.*, vol. 64, no. 9, pp. 4350–4356, Sep. 2015.

[31] C. Qian, J. Wu, Y. R. Zheng, and Z. Wang, "Simplified parallel interference cancelation for underdetermined MIMO systems," *IEEE Trans. Veh. Technol.*, vol. 63, no. 7, pp. 3196–3208, Sep. 2014.

[32] S. Brandes, U. Epple, S. Gligorevic, M. Schnell, B. Haindl, and M. Sajatovic, "Physical layer specification of the L-band digital aeronautical communications system (L-DACS1)," in *Proc. Integr. Commun. Navigat. Surveill. Conf.*, May 2009, pp. 1–12.

[33] M. Mostafa, N. Franzen, U. Epple, and M. Schnell, "Improving coding scheme of LDACS in the reverse link," in *Proc. IEEE/AIAA 34th Digit. Avionics Syst. Conf. (DASC)*, Sep. 2015, pp. 2C2-1–2C2-8.

YUAN HE (S'14) received the B.Eng. and M.S. degrees in communication and information engineering from Chongqing University, Chongqing, China. He is currently pursuing the Ph.D. degree with Southeast University, Nanjing, China. His research interests include mobile communications, coded modulation, and deep learning.

MING JIANG (S'06–M'07) received the B.Sc., M.S., and Ph.D. degrees in communication and information engineering from Southeast University, Nanjing, China, in 1998, 2003, and 2007, respectively. He is currently an Associate Professor with the National Mobile Communications Research Laboratory, Southeast University. His research interests include coding and modulation technology.

CHUNMING ZHAO (M'93) received the B.Sc. and M.S. degrees from the Nanjing Institute of Posts and Telecommunications, in 1982 and 1984, respectively, and the Ph.D. degree from the Department of Electrical and Electronic Engineering, University of Kaiserslautern, Germany, in 1993.

He is currently a Professor and the Vice Director of the National Mobile Communications Research Laboratory. His research interests include communication theory, coding/decoding, mobile communications, and VLSI design. He received the First Prize of the National Technique Invention of China, in 2011. He was a recipient of the Excellent Researcher Award from the Ministry of Science and Technology, China.